catalysts

MDPI

Article

Effect of Capping Ligands for the Synthesis of Gold Nanoparticles and on the Catalytic Performance for the Oxidation of 5-Hydroxymethyl-2-furfural

Francesca Liuzzi [1,2], Alessia Ventimiglia [1,2], Alessandro Allegri [1,2], Elena Rodríguez-Aguado [3], Juan Antonio Cecilia [3], Ivan Rivalta [1,2,4], Nikolaos Dimitratos [1,2,*] and Stefania Albonetti [1,2,*]

1 Industrial Chemistry "Toso Montanari" Department, University of Bologna, Viale Risorgimento 4, 40136 Bologna, Italy; francesca.liuzzi7@unibo.it (F.L.); alessia.ventimiglia3@unibo.it (A.V.); alessandro.allegri2@unibo.it (A.A.); i.rivalta@unibo.it (I.R.)
2 Center for Chemical Catalysis-C3, Alma Mater Studiorum Università di Bologna, Viale Risorgimento 4, 40136 Bologna, Italy
3 Departamento de Química Inorgánica, Cristalografía y Mineralogía, Facultad de Ciencias, Universidad de Málaga, Campus de Teatinos, 29071 Málaga, Spain; aguadoelena5@gmail.com (E.R.-A.); jacecilia@uma.es (J.A.C.)
4 Laboratoire de Chimie UMR 5182, ENSL, CNRS, 46 allée d'Italie, 69364 Lyon, France
* Correspondence: nikolaos.dimitratos@unibo.it (N.D.); stefania.albonetti@unibo.it (S.A.)

Abstract: Different series of Au on carbon catalysts were prepared via sol-immobilization to investigate the role of polymers (polyvinylpyrrolidone PVP, polyethylene glycol PEG and polyvinyl alcohol PVA), employed as gold nanoparticle (NP) stabilizers, on catalyst properties and on catalytic activity. The synthesized materials were widely characterized with several techniques (DLS, XRD, TEM and XPS) and used as catalysts in the 5-hydroxymethylfurfural (HMF) oxidation to produce 2,5-furandicarboxylic acid (FDCA). The obtained results clearly demonstrated the PVA leading to the formation of smaller and more active NPs. On the contrary, polyethylene glycol was shown to affect gold exposure and, as a consequence, to reduce the catalyst activity due to steric effects while PVP-based catalysts presented bigger and more covered Au NPs. The investigation on the reusability of the catalysts demonstrated the presence of a significant deactivation on all prepared materials, but the presence of higher amounts of polymer seems to have a positive effect on catalyst stability even if associated with lower reactivity. Computational studies have provided interesting information on the NP-polymer interactions and consequently on the catalytic activities.

Keywords: gold nanoparticles; stabilizer effect; polymers; HMF oxidation; sol-immobilization; DFT; cluster

Citation: Liuzzi, F.; Ventimiglia, A.; Allegri, A.; Rodríguez-Aguado, E.; Cecilia, J.A.; Rivalta, I.; Dimitratos, N.; Albonetti, S. Effect of Capping Ligands for the Synthesis of Gold Nanoparticles and on the Catalytic Performance for the Oxidation of 5-Hydroxymethyl-2-furfural. *Catalysts* **2023**, *13*, 990. https://doi.org/10.3390/catal13060990

Academic Editor: Sara Fulignati

Received: 12 May 2023
Revised: 2 June 2023
Accepted: 6 June 2023
Published: 9 June 2023

1. Introduction

Nanoparticles-based materials have attracted significant interest in the last few decades on account of their potential employment in several fields, such as medicine, biology, pollution remediation and catalysis [1–6]. The decrease in size of metal nanoparticles (NPs) corresponds to a higher surface-to-volume ratio and to a superior number of low coordinated atoms [7]. Due to these and other peculiar properties, metal NPs have shown considerable catalytic performances that are frequently in contrast with the bulk material: for instance, while bulk gold is an inert metal [8], gold nanoparticles are promising catalysts [9]. Since the first detection of these systems, reactivity in the CO oxidation at low temperature [10], gold-based catalysts have been studied for various catalytic applications, such as oxidation of alcohols and polyols [11,12], selective hydrogenation of alkynes [13] and many other organic reactions [14].

Concerning the use of nanoparticles-based catalysts, it is well documented that features such as the paracrystalline structure of the surface, shape and size of NPs can greatly

influence the catalytic activity [15–19]. Several methodologies can be used to control the dimensions of the NPs; for example, their deposition on a solid carrier effectively prevents their agglomeration [14,20]. To better control these characteristics, colloidal methods can also be adopted for the synthesis of the catalysts: a colloidal suspension is prepared, using stabilizers to limit crystal growth, and immobilized on a support material or applied directly as a catalyst. Therefore, metal NPs are coated by a capping ligand, in order to lower the surface energy and prevent aggregation, but, when the stabilizer is not removed, its presence can highly affect catalytic performance. It is widely reported that the stabilizer molecules can entirely or partially block the access to the metal surface of the nanoparticles, decreasing the detected activity of the catalyst [21,22]. Nevertheless, the steric and electronic effects of the stabilizers can also modify the catalytic surface, improving the performance of the catalyst [23]. As a consequence, nanoparticle-based stabilizers and their role in catalytic applications are becoming more important during catalyst design and several studies are beginning to focus on this topic [24,25].

In their work, Yang et al. [26] prepared Au/TiO_2 catalysts with different stabilizing agents (sodium acrylate (NaA), polysodium acrylate (PNaA), poly(vinyl alcohol) (PVA), and poly(vinyl pyrrolidone) (PVP)) and tested them in the CO oxidation. Comparing the results with Au/TiO_2 catalyst prepared without any capping ligand, they observed how the nature of PVA- and PVP-based samples have a negative impact in terms of catalytic activity. Despite that the catalyst without a stabilizer had larger Au NPs, 5.4 nm compared to 4.7 nm and 3.6 nm of the Au/TiO_2-PVA and PVP samples, its activity was higher. On the other hand, the Au/TiO_2 (NaA) and Au/TiO_2 (PNaA) had enhanced activity attributed to a higher number of defective gold surface sites, highlighting the importance of considering the physicochemical properties of the stabilizer because the choice and nature of stabilizer can affect the morphology and the reactivity of NPS-based catalysts. Garcia et al. [27] prepared Rh nanoparticles for a hydroformylation reaction and demonstrated that using triphenylphosphine (PPh_3) as a direct stabilizer of the NPs led to higher activity and stability against CS_2 poisoning compared with the sample prepared with tetraoctylammonium bromide (TOAB), which needs the presence of an external ligand to be activated. Furthermore, García-Aguilar et al. [28] studied the PVP effect on Pd NPs for formic acid decomposition, and they proved the strong influence of the polymer on both sites' accessibility and on the electronic properties of the metal surface.

In the field of biomass valorization, supported gold nanoparticles have been found to be promising catalysts for the oxidation of 5-hydroxymethyl-2-furfural (HMF) [29,30]. HMF, produced from glucose or fructose dehydration [31,32], is generally accepted to be one of the most versatile compounds derived from biomass [33]. A variety of furanic and non-furanic derivatives, with applications in polymers, fuels and the pharmaceutical industry [34–36], can be synthesized from this precursor. Particularly, 2,5-furandicarboxylic acid (FDCA) can be produced from the HMF oxidation [37,38]. FDCA is a noteworthy compound proposed as a possible biomass-derived substitute for terephthalic acid, the monomer used in the synthesis of polyethylene terephthalate (PET), for the production of its furan-based analogue, poly(ethylene furanoate) (PEF), and a series of other bio-based polymers [39,40]. In recent decades, the HMF oxidation to FDCA has been widely studied, and several catalysts and reaction conditions have been investigated in recent years to improve product selectivity [41–43]. In particular, many studies have been conducted on Au-based catalysts to search for the best support and reaction conditions [44–46].

On this basis, the main purpose of this paper is to study how polymeric stabilizers can affect catalytic performance in terms of activity selectivity and the stability of gold nanoparticles supported on activated carbon (AC) for HMF oxidation. This work is especially focused on a comparison between the catalytic activities of Au nanoparticles, prepared through sol-immobilization using three different commercial polymers as stabilizer agents: polyvinylpyrrolidone (PVP), polyethylene glycol (PEG) and polyvinyl alcohol (PVA). These three polymers have different structural properties, thus each stabilizer affects

the preparation of the supported NPs and, particularly, the catalytic performance as has been shown previously [47–51].

2. Results and Discussion

2.1. Catalysts Characterization

Three series of gold-based catalysts were prepared using commercial polymers (PVA, PEG, PVP) as NPs stabilizers, varying for each series the Au/Polymer weight ratio from 0.3 to 2.4, in order to study the effect of the polymer on the morphology of the catalyst and eventually on catalytic performances. The colloidal suspensions of gold were immobilized on activated carbon and the synthesized catalysts were identified by a name such as "Au/AC_PVA_0.3", specifying firstly the catalyst, secondly the stabilizing polymer, and lastly the Au/Polymer weight ratio. All the final fresh and used catalysts were completely characterized in previous works [47,49,50] using different techniques such as UV-Vis spectroscopy, XRD, DLS, ELS, XPS and TEM, and the data are reported in the Supplementary Information (from Figures S1–S14 and Tables S1–S3). A new characterization of the spent catalysts for the studied reaction is presented in the section concerning the reusability of the samples.

In Table 1 the list of synthesized catalysts is reported, along with their main relevant characteristics to better understand the role of the polymeric stabilizer.

Table 1. List of all the tested catalysts along with their characteristics: type of stabilizing agent, polymer:Au weight ratio, TEM mean nanoparticle size and percentage of Au on the catalyst surface obtained from XPS analysis.

Sample	Employed Polymer	Polymer:Au Weight Ratio	Au on Surface [at%]	Au NPs TEM Diameter (nm)
Au/AC _0	None	0	2.61	7.9 ± 6.3
Au/AC_PVA_0.3	PVA	0.3	3.48	4.3 ± 3.6
Au/AC_PVA_0.6	PVA	0.6	2.80	2.7 ± 1.6
Au/AC_PVA_1.2	PVA	1.2	2.40	2.6 ± 2.1
Au/AC_PVA_2.4	PVA	2.4	1.81	2.4 ± 1.2
Au/AC_PEG_0.3	PEG	0.3	0.84	5.3 ± 2.0
Au/AC_PEG_0.6	PEG	0.6	1.95	5.6 ± 2.2
Au/AC_PEG_1.2	PEG	1.2	1.52	5.9 ± 2.3
Au/AC_PEG_2.4	PEG	2.4	1.09	6.4 ± 2.2
Au/AC_PVP_0.3	PVP	0.3	1.43	5.5 ± 3.6
Au/AC_PVP_0.6	PVP	0.6	1.17	5.6 ± 3.9
Au/AC_PVP_1.2	PVP	1.2	0.15	7.4 ± 4.7
Au/AC_PVP_2.4	PVP	2.4	0.12	8.4 ± 4.9

The series of selected catalysts have been characterized extensively and the results have been discussed in detail in our previous studies using a number of characterization techniques [47]. The DLS and ELS analyses, reported in Figures S13 and S14, show different trends depending on the choice of capping agent. While the influence of temperature on zeta potential and hydrodynamic diameter is not noticeable for PVP- and PEG-stabilized NPs, Au-PVA0.6 sol displays a significant influence of the temperature on its properties. In a previously published paper [48], this was associated with the detachment of PVA from the Au surface and was not observed for PEG and PVP.

According to the results obtained from the TEM and XPS analysis, the comparison between the TEM diameter and the exposed gold surface shows how the nanoparticle size could affect the availability of gold on the surface. In particular, this comparison between the different samples exhibits a general trend where the lower mean Au nanoparticle size leads to an increase in the gold exposure on the catalyst surface. However, the chemical nature of the polymer affects the gold availability. Concerning the use of PVA as a stabilizing agent, the smallest nanoparticles prepared with PVA possess a lower amount of

gold available on the surface because of the higher polymer coverage. An increase in the amount of PVP leads to a counterintuitive growth of Au mean diameter and also to greater coverage of the active sites. PEG-based samples have a similar trend regarding the diameter of the gold; however, this polymer does not affect the gold exposure in a drastic way.

2.2. Catalytic Tests

Each catalyst was tested in the oxidation of 5-hydroxymethyl-2-furfural (HMF) to 2,5-furandicarboxylic acid (FDCA). The catalytic tests for the oxidation of HMF in the liquid phase were conducted at 70 °C for 4 h, with a HMF:Au:NaOH molar ratio of 1:0.01:4 and an oxygen pressure of 10 bar, using water as the solvent. These are the optimized experimental conditions based on our previous works [45,48,52]. In order to verify that these reaction conditions are also optimal for these kinds of catalytic systems, we used the reference catalyst Au/AC_PVA_0.6 to study different experimental conditions. The effect of the NaOH was studied, and the obtained results are reported in Figure S15 and demonstrate that a molar ratio 1:4 = HMF:NaOH permitted reaching the higher FDCA selectivity. A study on the O_2 pressure (Figure S18) showed that in the range of 10–20 bar, the catalytic results did not change; the oxygen dissolved in water does not pose a limit for the reaction at these pressures. To confirm that no external diffusional limitations affect the catalytic results, several experiments were carried out by changing the stirring rates (Figure S16) over the Au/AC_PVA_0.6 sample. At 150 rpm, an important carbon loss (higher than 10%) was observed, but it disappeared after increasing the stirring rate to 300 and 600 rpm. Low stirring rates probably avoid a proper diffusion of HMF to the active sites, promoting its degradation and leading to the formation of by-products. Blank tests were performed in the absence of a catalyst and on activated carbon alone as the chosen support. These tests confirmed that in the absence of gold, the only reaction that occurred was HMF degradation, according to previous work [52]. On the contrary, the presence of a gold-based catalyst promoted the HMF oxidation to 5-Hydroxymethylfurancarboxylic acid (HMFCA), as reported in Scheme 1. It was not possible to detect the presence of the HMFCA parallel product, 2,5-Diformylfuran (DFF): its formation is not favored in such basic conditions, because the aldehydic group of HMF undergoes the attack of a hydroxyl ion to form a geminal diol [53]. The HMFCA oxidation leads to the formation of 5-formyl-2-furancarboxylic acid (FFCA), which is rapidly oxidized to FDCA. Since this last step occurs quickly, while the FFCA formation is the rate-determining step, the product was often detected in small amounts [54].

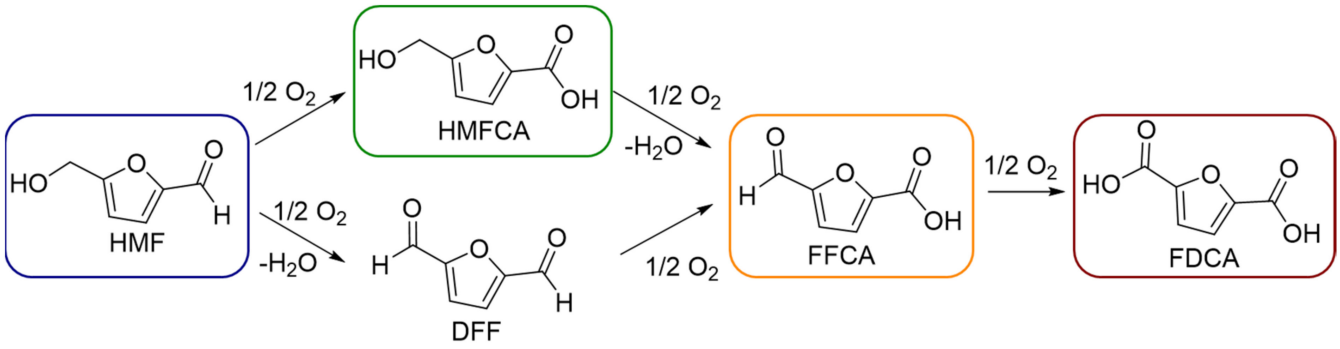

Scheme 1. The reaction pathway for the selective oxidation of HMF. The reaction pathway occurring on gold NPs is highlighted by colored boxes.

In Figure 1, the results obtained from the catalytic tests on the HMF oxidation are reported as a function of the polymer:Au weight ratio, showing the effect of the amount of polymer on the catalytic activity. HMF conversion was complete for each test, thus FDCA selectivity was used as a measure of the overall catalytic performance of the catalysts (Figure S17).

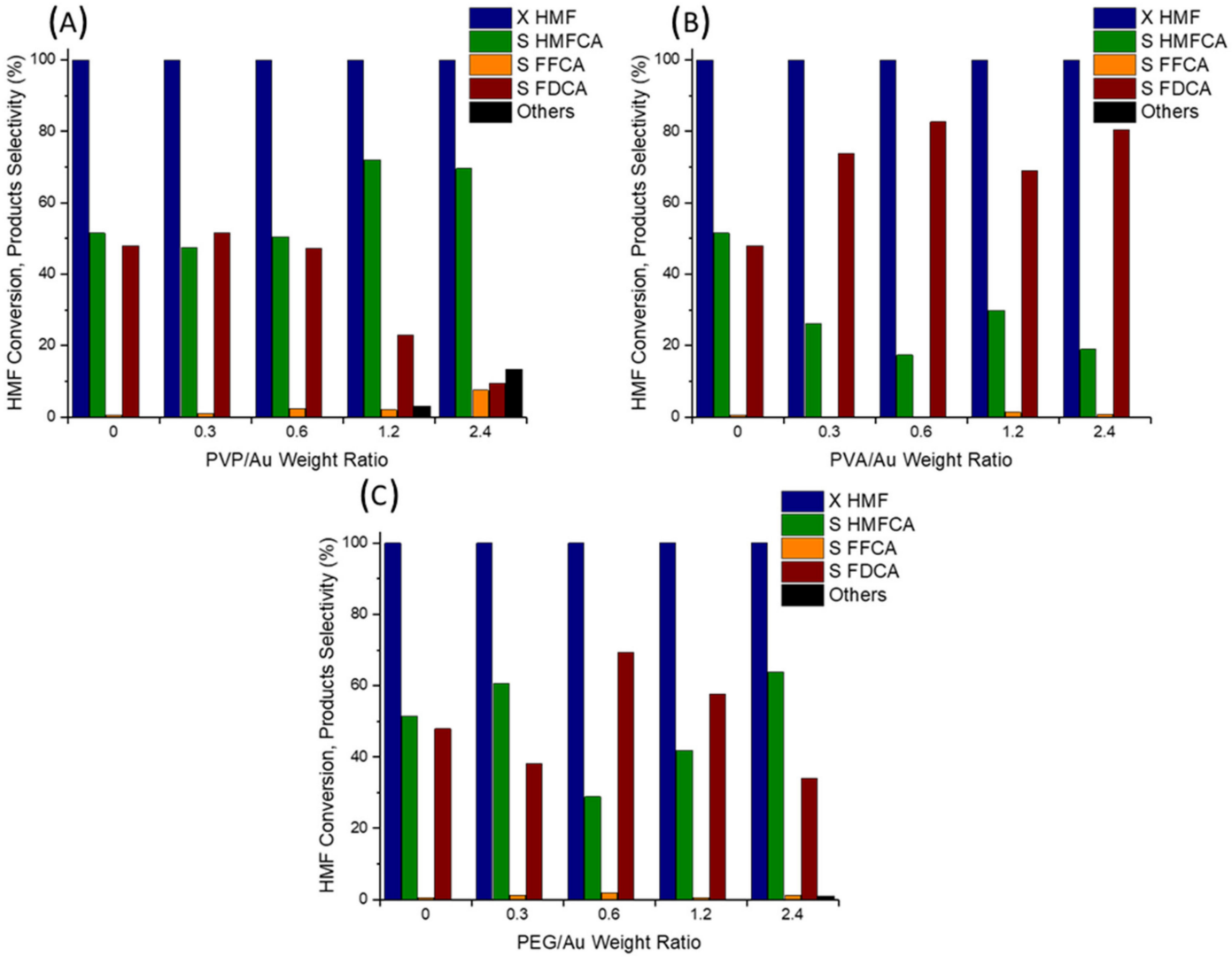

Figure 1. The catalytic results for the PVP-based catalysts (**A**), PVA-based catalysts (**B**) and PEG-based catalysts (**C**). Reaction conditions: 70 °C, 4 h, 10 bar O_2, HMF:Met:NaOH = 1:0.01:4.

When PVA is the chosen stabilizer, an increase in PVA/Au weight ratio leads to a significant increase in FDCA selectivity, from 50% in the absence of PVA to a maximum of 80% in the presence of a 0.6 PVA/Au weight ratio. PVA-stabilized catalysts presented the highest catalytic performances, while PVP-Au and PEG-Au samples generally showed lower FDCA selectivity at a similar polymer/Au weight ratio. In particular, when gold NPs are stabilized with PVP, catalysts with a lower amount of polymer (0.3–0.6) and without the stabilizer had similar performances, while higher amounts of PVP led to less active catalysts. When the PVP:Au weight ratio is equal to 2.4, the FDCA production is lower than the formation of by-products, due to a low catalytic activity. This behavior was already observed for the reaction of furfural oxidation in a previous study [50]; PEG-stabilized catalysts generally have lower performance rates compared to the PVA-Au samples, and the highest activity is reached when the stabilizer to Au weight ratio is 0.6.

Since a large amount of stabilizer clearly affects catalytic performances, especially for the PEG- and PVP-based samples, a study on the reaction time and temperature has been carried out on the three catalysts with a polymer:Au weight ratio of 0.6 as the preferred choice (Figures S19–S24). Figure 2 summarizes the effect of reaction time in the range of 0–4 h and the reaction temperature from 30 °C to 110 °C for the transformation of HMFCA to FDCA for the series of catalysts presented.

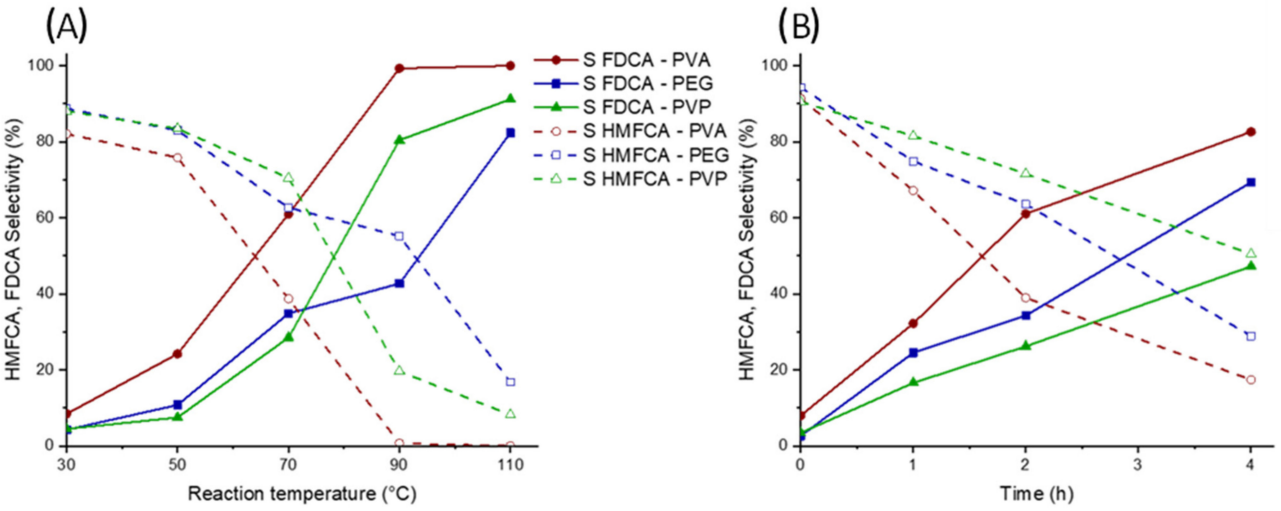

Figure 2. (**A**) The effect of the reaction temperature for catalysts with Polymer:Au weight ratio of 0.6 (2 h, 10 bar O_2, HMF:Met:NaOH = 1:0.01:4); (**B**) The effect of the reaction time for catalysts with Polymer:Au weight ratio of 0.6 (70 °C, 10 bar O_2, HMF:Met:NaOH = 1:0.01:4). The HMF conversion was 100% in all cases.

HMFCA is one of the reaction intermediates, and further oxidation of HMFCA to FDCA is possible via the formation of FFCA. Due to the presence of the hydroxyl group in the HMFCA, the oxidation of this intermediate to FFCA is the rate-determining step of the reaction [44]. It is evident that as the temperature increases HMFCA can be further oxidized to FDCA at higher rates above 60 °C. Moreover, considering the effect of the stabilizer, it can be seen that when PVA is chosen as the stabilizer, the FDCA selectivity is higher, whereas the PVP and PEG-Au supported nanoparticles show a significantly lower selectivity to FDCA below 90 °C. These results demonstrate that the interactions of the various stabilizers with the Au surface sites are different, and when PVA is used, the interaction is weaker, since at a lower reaction temperature it is possible to facilitate the formation of FDCA. In the case of PVP and PEG-Au supported nanoparticles, it is evident that the improvement of FDCA selectivity as the reaction temperature is increased. In particular, when the reaction temperature is increased to 110 °C, the difference in terms of FDCA selectivity of the PVA, PVP and PEG-Au supported nanoparticles is smaller, indicating that a higher reaction temperature facilitates the desorption of the stabilizer from the active site, especially in the case of PVP and PEG-Au supported nanoparticles.

2.3. Characterization of Catalysts for Evaluating the Difference in the Catalytic Activity

In Figure 3, the FDCA selectivity has been plotted as a function of Au mean particle size and Au surface exposure. Considering the characterization data, a good correlation between catalytic performances, Au mean particle size and the percentage of surface Au can be observed.

In previous work, Megías-Sayago et al. [55] already observed that the product selectivity and the carbon balance of the HMF oxidation depend on the gold nanoparticles' dimensions due to a higher exposure of the (100) face when the NPs are smaller. In this case, according to the catalytic tests and the results of the TEM analysis, a decrease in average Au nanoparticle size has a positive influence that increases the selectivity to FDCA (Figure 3A). The catalyst prepared without employing a polymeric stabilizer led to a ca. 50% FDCA selectivity and did not show a particular increase in terms of Au particle size, thanks to the presence of the reagents counterions during the colloidal suspension preparation. In the case of PVP-Au catalysts, a counter-intuitive growth in the diameter of the NPs can be observed when the amount of polymer increases; higher amounts of this polymer can probably affect the synthesis of the nanoparticles. However, a good correlation with the FDCA selectivity can be noted: when the nanoparticles increase in size, the catalyst activity

decreases. In addition, the catalytic results are well correlated with the percentage of the Au surface exposure (Figure 3B), and a higher amount of PVP not only led to the formation of bigger NPs but also covered the Au surface, resulting in a lower surface Au percentage and consequently less active catalysts. Instead, different PEG:Au weight ratios did not influence the NPs preparation significantly, all the PEG-based samples showed similar dimensions, but also in this case, an increase in stabilizer to Au weight ratio above 0.6 led to a decrease in Au exposure and in the selectivity to FDCA. All the catalysts with PVA as the chosen stabilizer presented smaller and more active nanoparticles. In terms of surface Au exposure and PVA coverage, the influence was not significant and the correlation with the catalytic results was not strong. This can be caused by a stabilizer removal from the catalyst surface during the 4 h of reaction: above 60 °C, the amount of PVA on the surface of Au nanoparticles could be reduced due to the higher degree of solubilization in the reaction medium [48]. Therefore, the availability of gold surface sites can be increased "in situ", even when a higher amount of PVA was used during the synthesis of the Au nanoparticles.

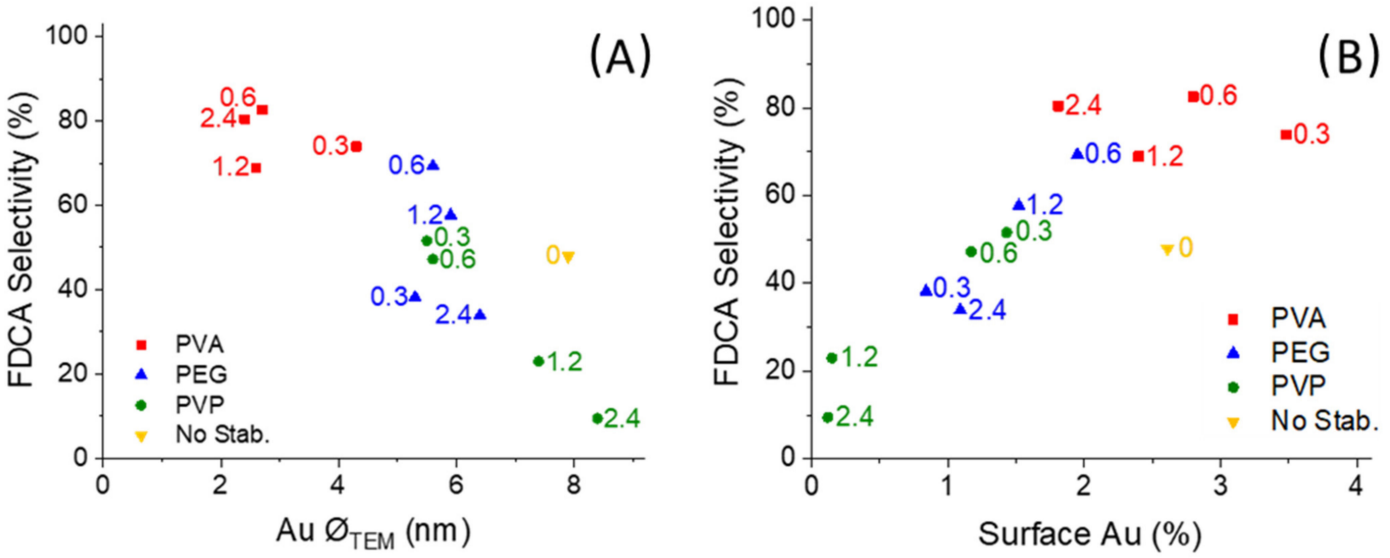

Figure 3. (**A**) The correlation between catalytic performances and Au mean particle size for the different catalysts. (**B**) T correlation between catalytic performances and surface Au percentage (XPS) for the different catalysts. All catalysts led to 100% HMF conversion.

2.4. Catalyst Reusability

The reusability of the three catalysts with polymer:Au ratio of 0.6 was studied carrying out subsequent reaction cycles on each sample. For these tests, the reaction time was decreased to 2 h in order to better evaluate possible changes in the catalyst behavior. The obtained results on the three catalysts are reported in Figure 4.

All the synthesized catalysts exhibited a similar trend: after the second use, the catalytic activity decreased significantly, in good agreement with the results reported in the literature on the low stability of gold NPs for the HMF oxidation reaction [45,46]. Concerning the PVP-based sample, during the third use, the catalyst was completely deactivated, the only HMF degradation reaction, which led to the formation of humins, and the reaction solution was dark red (Figure S25). The PEG-Au-supported nanoparticles showed a similar behavior: in the third test the FDCA selectivity was <5% and a significant amount of by-products formed, and the catalyst was no longer active. When PVA was chosen as the stabilizer, the FDCA selectivity was generally higher, but also in this case the catalyst deactivation was notable. The causes of catalyst deactivation were investigated with TEM and XPS analysis on the spent catalysts (Tables 2 and S3). All the spent samples presented a general growth of the Au nanoparticles in addition to a reduction in the gold surface exposure. The decrease in the percentage of surface gold could be caused by the NPs aggregation and fouling due to the formation of humins. Active phase leaching can be

excluded. A significant amount of gold was not detectable through MP-AES analysis on post-reaction solutions. Moreover, to exclude the Au leaching, a test of 4 h removing the catalyst after 1 h of reaction was carried out on the PVA-based sample (Figure S26). These results indicate that the detachment of the polymer from the surface of the NPs, combined with weak metal-supported interactions and relatively high reaction temperature, increases the mobility of the nanoparticles on the catalyst surface, causing their coalescence [56,57]. The selectivity of the products did not change after the last 3 h without the catalyst, suggesting the absence of Au NPs in the solution. To verify that the interaction between FDCA and the gold surface is not the cause of the catalyst deactivation, some experiments were conducting adding different amounts of this product at the beginning of the reaction (Figure S27). From the obtained results, it was possible to confirm that the presence of FDCA did not lead to the catalyst deactivation; in fact, the HMF conversion and products selectivity did not change when FDCA was added.

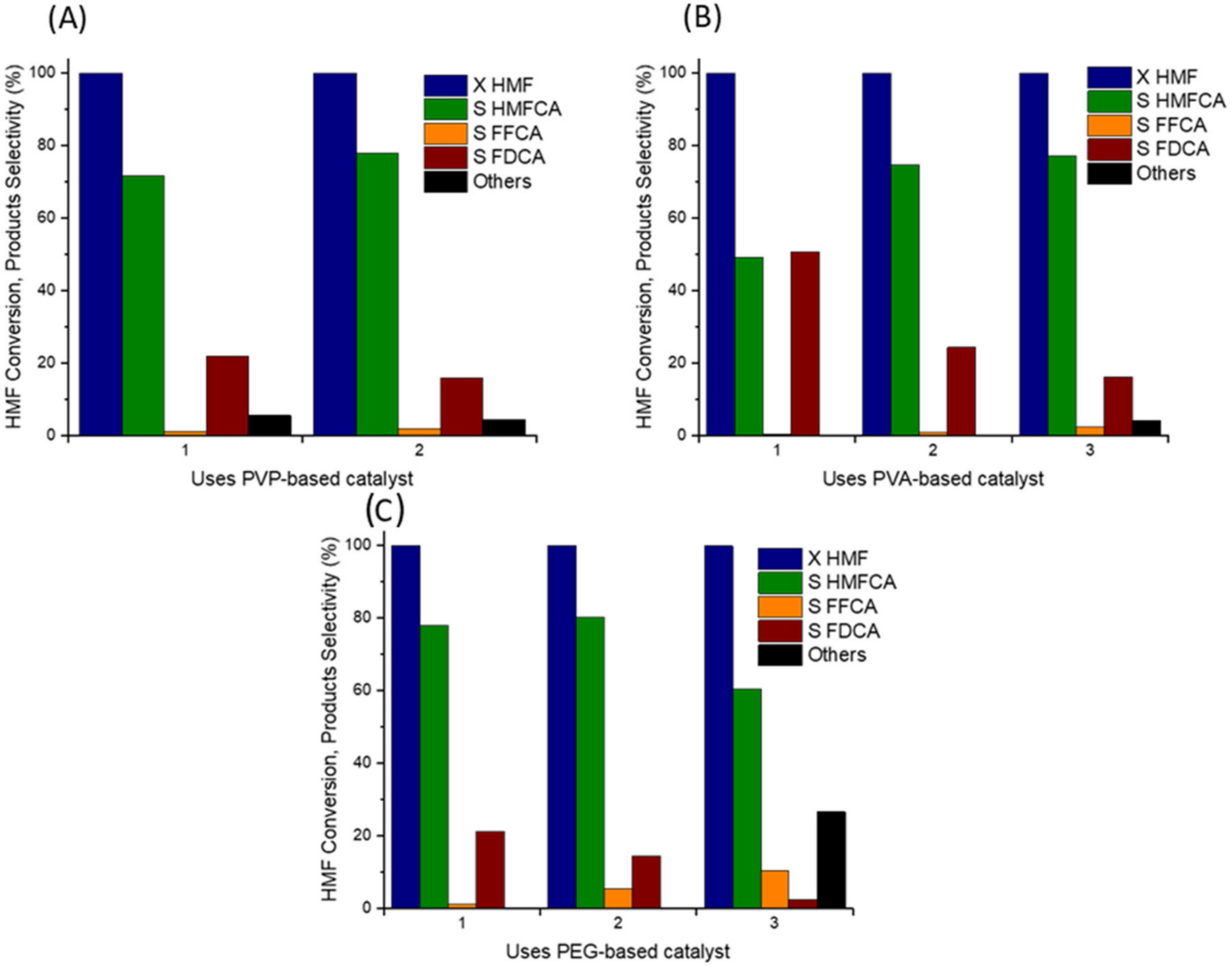

Figure 4. Reusability tests on the catalysts with PVP (**A**), PVA (**B**) and PEG stabilizers (**C**) with a polymer:Au weight ratio of 0.6. Reaction conditions: 70 °C, 2 h, 10 bar O_2, HMF:Met:NaOH = 1:0.01:4.

Table 2. A list of all the fresh and spent samples employed to study the catalyst stability along with TEM nanoparticles size and percentage of Au on the catalyst surface obtained from XPS analysis.

Sample	Au on Surface [at%]	Au NPs TEM Diameter (nm)
Au/AC_PVA_0.6	2.80	2.7 ± 1.6
Au/AC_PVA_0.6 3 uses	0.18	20 ± 10
Au/AC_PVA_2.4	1.81	2.4 ± 1.2
Au/AC_PVA_2.4 3 uses	0.24	9.4 ± 5.7
Au/AC_PEG_0.6	1.95	5.6 ± 2.2
Au/AC_PEG_0.6 3 uses	0.68	8.5 ± 4.9
Au/AC_PEG_2.4	1.09	6.4 ± 2.2
Au/AC_PEG_2.4 3 uses	0.71	9.9 ± 4.6
Au/AC_PVP_0.6	1.17	5.6 ± 3.9
Au/AC_PVP_0.6 3 uses	0.25	9.1 ± 5.4

For a better understanding of the influence of the stabilizer agent on the catalyst stability, the reusability tests were carried out at a higher polymer-to-Au weight ratio, using as reference samples the Au/AC_PVA_2.4 and Au/AC_PEG_2.4 catalysts (complete results are reported in Figure S28). The obtained results were compared with those of the catalysts with a polymer/Au weight ratio of 0.6 (Figure 5). The PVP-based catalysts with higher amounts of polymer were not tested due to their low activity after a single reaction cycle of 4 h.

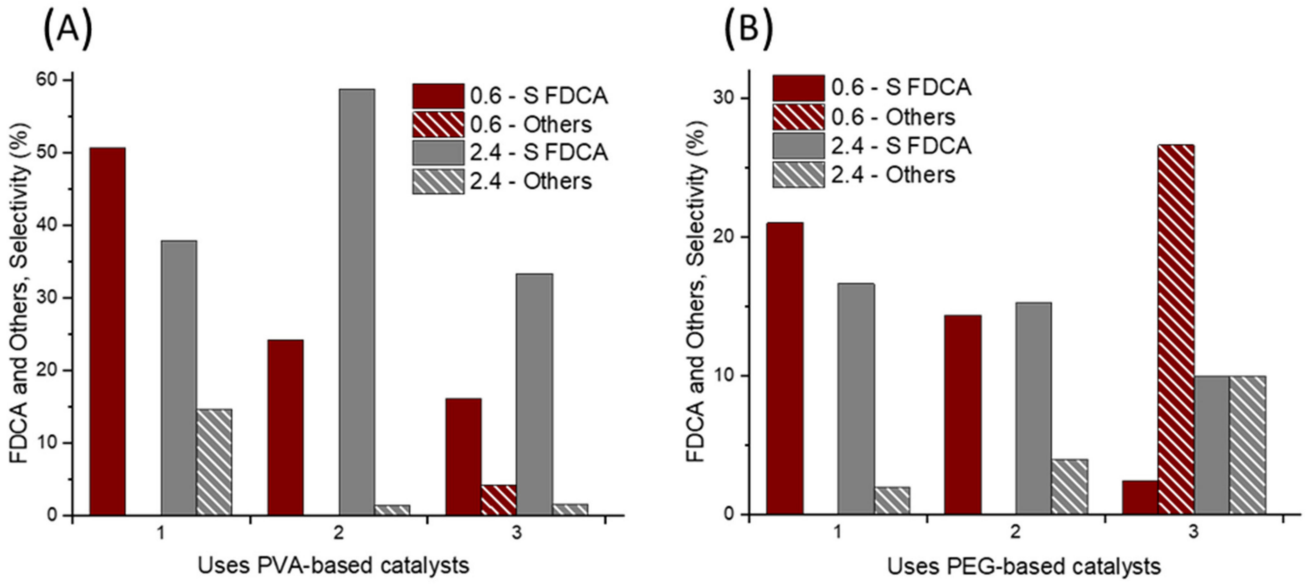

Figure 5. A comparison between the reusability tests for the Au/AC_PVA_0.6 and Au/AC_PVA_2.4 catalysts (**A**) and for the Au/AC_PEG_0.6 and Au/AC_PEG_2.4 catalysts (**B**). Reaction conditions: 70 °C, 2 h, 10 bar O_2, HMF:Met:NaOH = 1:0.01:4.

In general, the catalysts with a higher amount of polymer showed better stability compared with the catalysts with a lower amount of polymer. Concerning the PEG-based samples (Figure 5A), the FDCA selectivity slowly decreased using the catalyst with a higher amount of polymer, from 17% to 11% after the third cycle, while it decreased from 22% to less than 5% on the Au/AC_PEG_0.6 catalyst. The higher accessibility to active sites,

when the lower stabilizer is employed, is probably responsible for the enhanced initial activity, but faster fouling through the three cycles was observed because the side reactions are also enhanced. On the contrary, better stability after 3 reactions was observed with a higher amount of PEG, despite the lower preliminary activity, showing the importance of the nature and concentration of the chosen and desired stabilizer.

For the Au/AC_PVA_2.4 sample (Figure 5B), the FDCA selectivity increased after a reaction cycle, reaching almost 60%, to decrease after the third cycle, while the activity loss was constant after each cycle on the other catalyst. PVA is known to be a stabilizer that can be washed away from the NPs surface at relatively low temperatures (>60 °C) [48]; therefore, the increase in activity after the first cycle could be attributed to the polymer removal from the active phase of the nanoparticle and, therefore, the increase in the concentration of the Au active sites.

Concerning the catalyst with a PVA:Au weight ratio of 0.6, the majority of the polymer amount on the surface of the catalyst probably solubilized during the first reaction cycle, thus increasing the catalytic activity but consequently leading to a less stable catalyst. Indeed, after three reaction cycles, the mean gold diameter increased from 2.7 nm to 20 nm (Figure 6) while the gold exposure drastically decreased, justifying the quick loss of activity. Conversely, higher amounts of stabilizer can partially block the active sites, also explaining the values of by-products selectivity near the 15% obtained from the first test on Au/AC_PVA_2.4, but after a reaction cycle enhanced FDCA selectivity was observed. In this case, after all tests, the Au NPs resulting growth was lower, since the higher amount of polymer prevents the aggregation of the nanoparticles, improving their stability. Therefore, it is crucial to find the delicate balance between the nature and concentration of the chosen polymeric stabilizer for maintaining catalytic performance and minimizing deactivation.

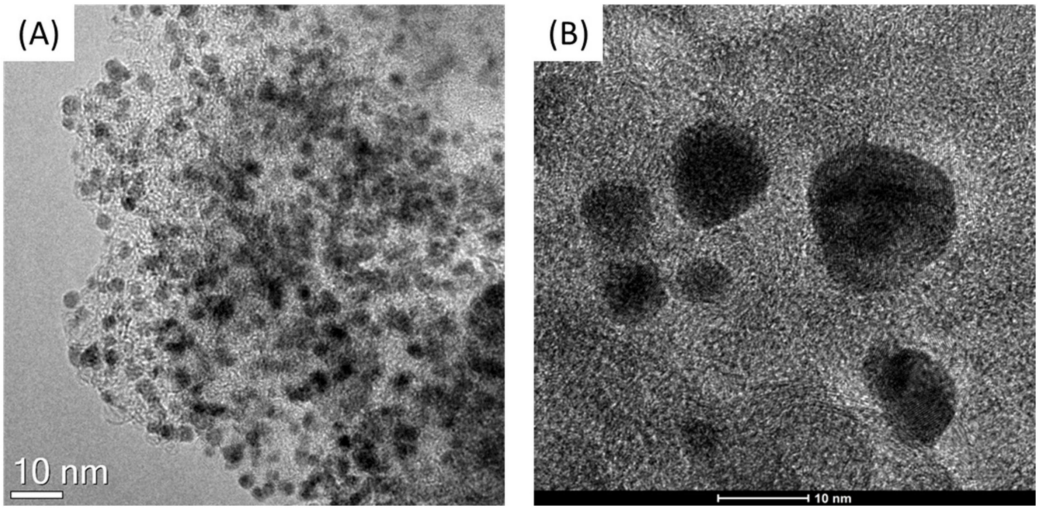

Figure 6. The TEM images of the fresh (**A**) and spent (**B**) catalyst Au/AC_PVA_0.6.

2.5. Interaction between Stabilizing Agents and Au NPs: A Computational Study

To better understand the interactions between the stabilizing agents and the Au NPs, we carried out a computational study based on density functional theory (DFT). As a model system for Au NPs, an Au_{55} amorphous cluster [58], with a size of ca. 1 nm was employed, since it was successfully used in a previous study on glucose oxidation reaction [47]. The adsorption of the three polymeric stabilizers was studied by considering the adsorption of their monomeric units.

Figure 7 shows the optimized structures of the PVA, PEG and PVP monomeric units adsorbed on a low-coordinated Au atom of the amorphous Au_{55} nanoparticle. The most stable surface interactions occur with O atoms of the polymeric monomers, i.e., with the hydroxyl group of PVA, the ether oxygen of PEG and the carboxylic group of PVP. The Au-O distances turned out to be 2.50 Å, 2.47 Å and 2.31 Å for PVA, PEG and PVP, respectively.

The PVA monomer, thus, appears to be the one bound least strongly to the nanoparticle, followed by PEG and PVP. This trend was also confirmed by the corresponding adsorption energies reported in Table 3.

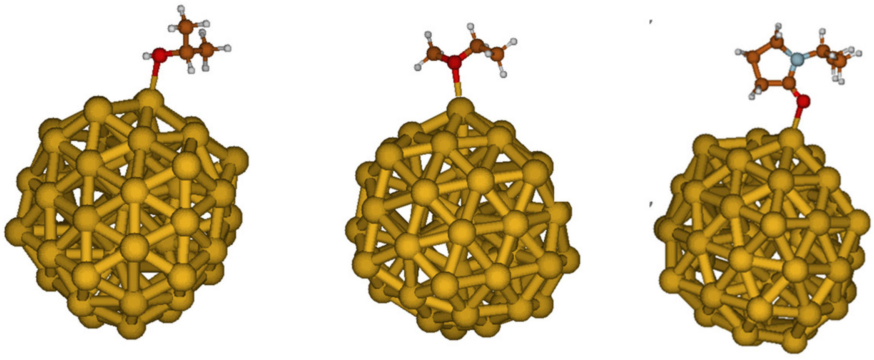

Figure 7. The DFT optimized structures of stabilizing agents (PVA on the left, PEG in the center and PVP on the right) adsorbed on the Au_{55} cluster model.

Table 3. Adsorption energies and Au-O distances of the three stabilizing agents on Au_{55}.

Stabilizing Agent	Eads (kCal/mol)	Distance Au-O (Å)
PVA	−28.7	2.50
PEG	−31.6	2.47
PVP	−36.8	2.31

Notably, the computed adsorption energies and optimized geometries of the adsorbed monomeric units of the stabilizing agents agree with the experimental observation that water washing of the PVA-stabilized NPs removes the polymer from the catalyst surface at relatively low temperatures more effectively than for PEG and PVP [48].

3. Materials and Methods

3.1. Materials

Tetrachlorauric acid ($HAuCl_4 \cdot 3H_2O$, Sigma Aldrich, Darmstadt, Germany), sodium borohydride (NaBH4, 99%, Sigma Aldrich), activated carbon NORIT SX1G, sulfuric acid (H_2SO_4, 96%, Sigma Aldrich) poly(vinyl alcohol) (PVA, MW 13,000–23,000 g mol^{-1}, hydrolyzed 87–89%, Sigma Aldrich), polyvinylpyrrolidone (PVP, MW 29,000 g mol^{-1}, Sigma Aldrich), polyethylenglycol (PEG, MW 8000 g mol^{-1}, Sigma Aldrich) were employed for the catalyst synthesis. For the catalytic tests, 5-hydroxymethylfurfural (AVA Biochem, Zug, Switzerland) and sodium hydroxide pellets (>98%, Sigma Aldrich) were used, and 2,5-furandicarboxylic acid, 5-hydroxymethyl-2-furancarboxylic acid, 5-formyl-2-furancarboxylic acid, and 2,5-diformylfuran (FDCA, HMFCA, FFCA) (Toronto Research Chemical, North York, ON, Canada) were employed as reference commercial species for HPLC analysis. The reactants and products quantification was conducted using an external calibration method.

3.2. Catalysts Preparation

The catalysts were prepared via sol-immobilization, using the following experimental protocol [47,50]. To prepare 1 g of the catalyst with a nominal metal loading of 1%wt, the desired amount of $HAuCl_4 \cdot 3H_2O$ (1.9 mmol) was dissolved in 390 of distilled H_2O, adding a precise volume of polymer (PVA, PVP, PEG, in aqueous solution 0.101 g mL^{-1}) as a stabilizing agent. After 3 min, an aqueous solution of $NaBH_4$ (Au:$NaBH_4$ = 1:5 mol/mol) was added to the gold and stabilizer solution, to form a red colloidal suspension of Au^0. The solution was left under stirring for 30 min; then the nanoparticles were immobilized by adding 0.99 g of the support (activated carbon, AC), and the solution was acidified at pH 2 by using sulfuric acid. After 1 h of stirring, the catalyst was filtered and washed with

distilled water to remove ionic species, until the washing water reached a neutral pH. After drying for a night at room temperature in a watch glass, the catalyst was treated at 80 °C in an oven for 4 h.

3.3. Characterization

The synthesized catalysts have been characterized by means of UV-Vis spectroscopy, DLS, XRD, TEM and XPS. The colloidal suspensions were characterized by dynamic light scattering (DLS) and electrophoretic light scattering (ELS) analysis, using a Malvern Panalytical (Malvern, UK) Zetasizer Nano ZS instrument. The DLS analysis was performed in a standard polystyrene cell at 25 °C (or at the desired temperature), while for the zeta potential analysis a capillary polycarbonate cell equipped with electrodes was utilized. On the colloidal suspensions was also performed UV-Vis analysis using an Agilent Cary 3500 UV-Vis Spectrometer. Powder X-ray diffraction (XRD) patterns were collected employing a Malvern Panalytical (Malvern, UK = X'PertPRO) X-ray diffractometer using a Cu radiation source (1.54 Å). To estimate the mean size of the NPs and their distribution, Transmission Electron Microscopy (TEM) analysis was performed using a Thermo Fisher (Waltham, MA, USA) FEI Talos F200x high-resolution transmission microscope. To prepare the samples, firstly the catalyst was suspended in ethanol and treated by ultrasound for 15 min; then a drop of the suspension was deposited on "quantifoil-carbon film" supported by a grid of Cu, dried at 120 °C and analyzed. A minimum of 400 NPs were measured to evaluate the nanoparticles' average size and size distribution. The XPS spectra were recorded with a Physical Electronic spectrometer (PHI Versa Probe II), using monochromatic Al Kα radiation (15 kV, 1486.6 eV) and a dual beam charge neutralizer for analyzing the core-level signals of the elements of interest. High-resolution spectra were recorded using a concentric hemispherical analyzer with a constant pass energy value of 29.35 eV, irradiating an analysis area of 100 μm in diameter. The binding energy was determined with a precision of ±0.1 eV, using as reference the C 1s signal 284.5 eV. The pressure in the analysis chamber was kept below 5–10 Pa. The SmartSoft-VP 2.10.4.1 software was used for the acquisition of analysis data. A Shirley-type background was subtracted from the signals. The spectra that were recorded were analyzed with Gauss-Lorentz-type curves to determine, with greater precision, the binding energy of the atomic levels of the different elements. Atomic concentration percentages of the characteristic elements were determined considering the corresponding area sensitivity factor for the different measured spectral regions.

3.4. 5-Hydroxymethylfurfural Oxidation Tests

The catalytic tests were carried out in a 100 mL PARR autoclave, with a mechanical stirrer (0–600 rpm) [52,59]. Standard reactions were performed at 70 °C, stirring the solution at 600 rpm for 4 h. Before starting the reaction, 25 mL of HMF aqueous solution with the necessary amount of catalyst and NaOH (HMF:Au:NaOH molar ratios of 1:0.01:4) was charged in the reactor. Then the autoclave was purged 3 times with 10 bar of oxygen and finally pressurized (10 bar). When the temperature reached the set point, the reaction began (t = 0). After the selected time of reaction, the autoclave was cooled down in an ice bath. To remove the catalyst, the reaction mixture was centrifugated and a sample was collected and diluted 1:5 before HPLC analysis. The analysis was performed with an Agilent Infinity 1260 liquid chromatograph equipped with an Aminex HPX-87H 300 mm × 7.8 mm column using 0.005 M H_2SO_4 as eluent. To calculate the concentration of each reactive species present in the reaction (HMF, HMFCA, FFCA, FDCA), an external calibration curve prepared using reference commercial samples was used. Conversion yields and selectivity were calculated according to the following equations:

$$HMF\ conversion\ (\%) = \frac{[HMF]_0 - [HMF]_F}{[HMF]_0} \times 100 \quad (1)$$

$$Product\ selectivity\ (\%) = \frac{Product\ moles}{HMF\ moles_0 - HMF\ moles_F} \times 100 \quad (2)$$

$$Product\ yield\ (\%) = \frac{Conversion \times Selectivity}{100} \quad (3)$$

3.5. Computational Studies

The model used for small Au NPs is an amorphous Au_{55} cluster previously reported elsewhere [47]. All structures were optimized at the DFT level using the hybrid B3LYP exchange–correlation functional [60–62] as implemented in the Gaussian16 package [63]. The effect of the solvent (water) has been taken into account using the polarizable continuum model [64]. The energy of adsorption was calculated using the following equation:

$$E_{ads} = E_{Au55\ +\ stabilizing\ agent} - E_{Au55} - E_{stabilizing\ agent} \quad (4)$$

The Stuttgart effective core potential was used for the Au atoms [65] to account for scalar relativistic effects, while for the atoms of the polymeric units (H, C, N and O) the 6–31G** basis set was employed [66]. Single-point calculations were performed using the larger basis set 6–311++G** [66] for the stabilizing agent of the atoms (H, C, N and O). The counterpoise correction was applied to account for the basis set superposition error [67].

4. Conclusions

The catalytic activity of several Au/AC samples, prepared employing different polymeric stabilizing agents (PVA, PEG and PVP), was investigated in this work. The selective oxidation of HMF to FDCA was used to better evaluate the role and influence of the stabilizer on the catalytic performance of Au nanoparticles. The catalytic results demonstrated that the nature and the amount of stabilizer had a significant impact not only on the catalysts' activity but also on their stability. When PVA was the chosen stabilizing agent, smaller and more active nanoparticles could be obtained, independently from the polymer:Au weight ratio. On the contrary, PEG- and PVP-based samples presented bigger and less active NPs when the polymer amount was increased. Computational studies on the adsorption of the polymer monomeric units on the Au_{55} cluster can explain the improved activity of the PVA-based catalysts. The monomer of PVA presented the lowest adsorption energy on the Au_{55} cluster and the longest Au-O bond, thus the polymer can be washed away from the gold surface at relatively low temperatures, increasing the number of free active sites during the reaction. Moreover, the studies on the catalysts' stability highlighted the importance of the stabilizer amount; in fact, catalysts with a 2.4 polymer:Au weight ratio presented a certain stability for two reaction cycles, while the activity of the catalysts with less polymer drastically decreased after the first reaction. These studies show the significance of investigating the nature of the stabilizer and its amount for improving catalyst activity and preserving its stability and therefore can open new scientific pathways for continuing research to optimize the use of preformed colloidal metal nanoparticles for a range of different catalytic applications in liquid and gas phase.

Supplementary Materials: The following supporting information can be downloaded at: https://www.mdpi.com/article/10.3390/catal13060990/s1, Figure S1. The correlation between mean particle size measured by TEM and the percentage of Au on surface (XPS analysis); Figure S2. UV-Vis spectra of Au NPs colloidal suspension with varying amounts of PVA as stabilizer; Figure S3. UV-Vis spectra of Au NPs colloidal suspension with varying amounts of PEG as stabilizer; Figure S4. UV-Vis spectra of Au NPs colloidal suspension with varying amounts of PVP as stabilizer; Figure S5. XRD patterns of Au/AC samples with different PVA:Au weight ratios; Figure S6. XRD patterns of Au/AC samples with different PEG:Au weight ratios; Figure S7. XRD patterns of Au/AC samples with different PVP:Au weight ratio; Figure S8. TEM images and particle size distributions of Au/AC_PVP_0.6 catalyst before and after two reaction cycles; Figure S9. TEM images and particle size distributions of Au/AC_PEG_0.6 catalyst before and after three reaction cycles; Figure S10. TEM images

and particle size distributions of Au/AC_PEG_2.4 catalyst before and after three reaction cycles; Figure S11. TEM images and particle size distributions of Au/AC_PVA_0.6 catalyst before and after three; Figure S12. TEM images and particle size distributions of Au/AC_PVA_2.4 catalyst before and after three reaction cycles; Figure S13. Temperature effect on zeta potential for the Au colloidal suspension stabilized with different polymers (PVA, PEG, PVP); Figure S14. Temperature effect on DLS diameter for the Au colloidal suspension stabilized with different polymers (PVA, PEG, PVP); Figure S15. Effect of the NaOH equivalent on the sample Au/AC_PVA_0.6; Figure S16. Effect of the stirring rate on the sample Au/AC_PVA_0.6; Figure S17. Correlation between catalytic performances and stabilizer to Au weight ratio for each catalyst series; Figure S18. Effect of the oxygen pressure on the 0.6 Polymer:Au weight ratio catalysts; Figure S19. Study on the reaction time. Catalyst: Au/AC_PEG_0.6; Figure S20. Study on the reaction temperature. Catalyst: Au/AC_PEG_0.6; Figure S21. Study on the reaction time. Catalyst: Au/AC_PVP_0.6; Figure S22. Study on the reaction temperature. Catalyst: Au/AC_PVP_0.6; Figure S23. Study on the reaction time. Catalyst: Au/AC_PVA_0.6; Figure S24. Study on the reaction temperature. Catalyst: Au/AC_PVA_0.6; Figure S25. Comparison of reaction solution after the first test on Au/AC_PVP_0.6 and after the third test; Figure S26. Leaching evaluation test; Figure S27. Effect of the FDCA in the starting reaction mixture; Figure S28. Reusability tests for the Au/AC_PVA_2.4 (A) and Au/AC_PEG_2.4 catalysts (B). Table S1. Mean crystallite size for Au/AC samples calculated from XRD analysis; Table S2. XPS Analysis for the synthesized catalysts; Table S3. XPS analysis on spent catalysts (after 3 uses).

Author Contributions: Conceptualization, S.A., N.D., A.A. and F.L.; methodology, F.L., A.V. and A.A.; software, I.R. and A.V.; validation, A.V., F.L. and E.R.-A.; formal analysis, E.R.-A. and J.A.C.; investigation, A.A., F.L. and A.V.; resources, S.A., N.D., I.R. and J.A.C.; data curation, F.L., A.V. and A.A.; writing—original draft preparation, S.A. and N.D.; writing—review and editing, F.L., A.V., N.D., S.A. and I.R.; visualization, A.A. and E.R.-A.; supervision, J.A.C., N.D., I.R. and S.A.; project administration, N.D. and S.A.; funding acquisition, N.D., I.R. and S.A. All authors have read and agreed to the published version of the manuscript.

Funding: This research received no external funding.

Data Availability Statement: Data are contained within the article.

Acknowledgments: IR gratefully acknowledges the use of HPC resources of the "Pôle Scientifique de Modélisation Numérique" (PSMN) of the ENS-Lyon, France. The authors thank the anonymous reviewers for their constructive comments.

Conflicts of Interest: The authors declare no conflict of interest.

References

1. Dykman, L.; Khlebtsov, N. Gold Nanoparticles in Biomedical Applications: Recent Advances and Perspectives. *Chem. Soc. Rev.* **2012**, *41*, 2256–2282. [CrossRef] [PubMed]
2. Sperling, R.A.; Rivera Gil, P.; Zhang, F.; Zanella, M.; Parak, W.J. Biological Applications of Gold Nanoparticles. *Chem. Soc. Rev.* **2008**, *37*, 1896. [CrossRef]
3. Savage, N.; Diallo, M.S. Nanomaterials and Water Purification: Opportunities and Challenges. *J. Nanoparticle Res.* **2005**, *7*, 331–342. [CrossRef]
4. Rosi, N.L.; Mirkin, C.A. Nanostructures in Biodiagnostics. *Chem. Rev.* **2005**, *105*, 1547–1562. [CrossRef] [PubMed]
5. Ndolomingo, M.J.; Bingwa, N.; Meijboom, R. Review of Supported Metal Nanoparticles: Synthesis Methodologies, Advantages and Application as Catalysts. *J. Mater. Sci.* **2020**, *55*, 6195–6241. [CrossRef]
6. Zhao, J.; Jin, R. Heterogeneous Catalysis by Gold and Gold-Based Bimetal Nanoclusters. *Nano Today* **2018**, *18*, 86–102. [CrossRef]
7. Burda, C.; Chen, X.; Narayanan, R.; El-Sayed, M.A. Chemistry and Properties of Nanocrystals of Different Shapes. *Chem. Rev.* **2005**, *105*, 1025–1102. [CrossRef] [PubMed]
8. Hashmi, A.S.K.; Hutchings, G.J. Gold Catalysis. *Angew. Chem. Int. Ed.* **2006**, *45*, 7896–7936. [CrossRef] [PubMed]
9. Hervés, P.; Pérez-Lorenzo, M.; Liz-Marzán, L.M.; Dzubiella, J.; Lu, Y.; Ballauff, M. Catalysis by Metallic Nanoparticles in Aqueous Solution: Model Reactions. *Chem. Soc. Rev.* **2012**, *41*, 5577. [CrossRef]
10. Haruta, M.; Kobayashi, T.; Sano, H.; Yamada, N. Novel Gold Catalysts for the Oxidation of Carbon Monoxide at a Temperature Far below 0 °C. *Chem. Lett.* **1987**, *16*, 405–408. [CrossRef]
11. Dimitratos, N.; Villa, A.; Prati, L.; Hammond, C.; Chan-Thaw, C.E.; Cookson, J.; Bishop, P.T. Effect of the Preparation Method of Supported Au Nanoparticles in the Liquid Phase Oxidation of Glycerol. *Appl. Catal. Gen.* **2016**, *514*, 267–275. [CrossRef]
12. Hutchings, G.J. Selective Oxidation Using Supported Gold Bimetallic and Trimetallic Nanoparticles. *Catal. Today* **2014**, *238*, 69–73. [CrossRef]

13. Yan, X.; Bao, J.; Yuan, C.; Wheeler, J.; Lin, W.-Y.; Li, R.; Jang, B.W.-L. Gold on Carbon and Titanium Oxides Composites: Highly Efficient and Stable Acetylene Hydrogenation in Large Excess of Ethylene. *J. Catal.* **2016**, *344*, 194–201. [CrossRef]
14. Corma, A.; Garcia, H. Supported Gold Nanoparticles as Catalysts for Organic Reactions. *Chem. Soc. Rev.* **2008**, *37*, 2096. [CrossRef] [PubMed]
15. Jin, L.; Liu, B.; Duay, S.; He, J. Engineering Surface Ligands of Noble Metal Nanocatalysts in Tuning the Product Selectivity. *Catalysts* **2017**, *7*, 44. [CrossRef]
16. Bell, A.T. The Impact of Nanoscience on Heterogeneous Catalysis. *Science* **2003**, *299*, 1688–1691. [CrossRef]
17. Zhou, X.; Xu, W.; Liu, G.; Panda, D.; Chen, P. Size-Dependent Catalytic Activity and Dynamics of Gold Nanoparticles at the Single-Molecule Level. *J. Am. Chem. Soc.* **2010**, *132*, 138–146. [CrossRef]
18. Laoufi, I.; Saint-Lager, M.-C.; Lazzari, R.; Jupille, J.; Robach, O.; Garaudée, S.; Cabailh, G.; Dolle, P.; Cruguel, H.; Bailly, A. Size and Catalytic Activity of Supported Gold Nanoparticles: An in Operando Study during CO Oxidation. *J. Phys. Chem. C* **2011**, *115*, 4673–4679. [CrossRef]
19. Jurkiewicz, K.; Kamiński, M.; Glajcar, W.; Woźnica, N.; Julienne, F.; Bartczak, P.; Polański, J.; Lelątko, J.; Zubko, M.; Burian, A. Paracrystalline Structure of Gold, Silver, Palladium and Platinum Nanoparticles. *J. Appl. Crystallogr.* **2018**, *51*, 411–419. [CrossRef]
20. Bujak, P.; Bartczak, P.; Polanski, J. Highly Efficient Room-Temperature Oxidation of Cyclohexene and d-Glucose over Nanogold Au/SiO_2 in Water. *J. Catal.* **2012**, *295*, 15–21. [CrossRef]
21. Villa, A.; Wang, D.; Veith, G.M.; Vindigni, F.; Prati, L. Sol Immobilization Technique: A Delicate Balance between Activity, Selectivity and Stability of Gold Catalysts. *Catal. Sci. Technol.* **2013**, *3*, 3036–3041. [CrossRef]
22. Quintanilla, A.; Butselaar-Orthlieb, V.C.L.; Kwakernaak, C.; Sloof, W.G.; Kreutzer, M.T.; Kapteijn, F. Weakly Bound Capping Agents on Gold Nanoparticles in Catalysis: Surface Poison? *J. Catal.* **2010**, *271*, 104–114. [CrossRef]
23. Baker, L.R.; Kennedy, G.; Krier, J.M.; Van Spronsen, M.; Onorato, R.M.; Somorjai, G.A. The Role of an Organic Cap in Nanoparticle Catalysis: Reversible Restructuring of Carbonaceous Material Controls Catalytic Activity of Platinum Nanoparticles for Ethylene Hydrogenation and Methanol Oxidation. *Catal. Lett.* **2012**, *142*, 1286–1294. [CrossRef]
24. Rossi, L.M.; Fiorio, J.L.; Garcia, M.A.S.; Ferraz, C.P. The Role and Fate of Capping Ligands in Colloidally Prepared Metal Nanoparticle Catalysts. *Dalton Trans.* **2018**, *47*, 5889–5915. [CrossRef]
25. Heuer-Jungemann, A.; Feliu, N.; Bakaimi, I.; Hamaly, M.; Alkilany, A.; Chakraborty, I.; Masood, A.; Casula, M.F.; Kostopoulou, A.; Oh, E.; et al. The Role of Ligands in the Chemical Synthesis and Applications of Inorganic Nanoparticles. *Chem. Rev.* **2019**, *119*, 4819–4880. [CrossRef]
26. Yang, N.; Pattisson, S.; Douthwaite, M.; Zeng, G.; Zhang, H.; Ma, J.; Hutchings, G.J. Influence of Stabilizers on the Performance of Au/TiO_2 Catalysts for CO Oxidation. *ACS Catal.* **2021**, *11*, 11607–11615. [CrossRef]
27. Garcia, M.A.S.; Ibrahim, M.; Costa, J.C.S.; Corio, P.; Gusevskaya, E.V.; dos Santos, E.N.; Philippot, K.; Rossi, L.M. Study of the Influence of PPh3 Used as Capping Ligand or as Reaction Modifier for Hydroformylation Reaction Involving Rh NPs as Precatalyst. *Appl. Catal. Gen.* **2017**, *548*, 136–142. [CrossRef]
28. García-Aguilar, J.; Navlani-García, M.; Berenguer-Murcia, Á.; Mori, K.; Kuwahara, Y.; Yamashita, H.; Cazorla-Amorós, D. Evolution of the PVP–Pd Surface Interaction in Nanoparticles through the Case Study of Formic Acid Decomposition. *Langmuir* **2016**, *32*, 12110–12118. [CrossRef]
29. Sang, B.; Li, J.; Tian, X.; Yuan, F.; Zhu, Y. Selective Aerobic Oxidation of the 5-Hydroxymethylfurfural to 2,5-Furandicarboxylic Acid over Gold Nanoparticles Supported on Graphitized Carbon: Study on Reaction Pathways. *Mol. Catal.* **2019**, *470*, 67–74. [CrossRef]
30. Zhang, Z.; Deng, K. Recent Advances in the Catalytic Synthesis of 2,5-Furandicarboxylic Acid and Its Derivatives. *ACS Catal.* **2015**, *5*, 6529–6544. [CrossRef]
31. Tacacima, J.; Derenzo, S.; Poco, J.G.R. Synthesis of HMF from Fructose Using Purolite®Strong Acid Catalyst: Comparison between BTR and PBR Reactor Type for Kinetics Data Acquisition. *Mol. Catal.* **2018**, *458*, 180–188. [CrossRef]
32. Morales-delaRosa, S.; Campos-Martin, J.M.; Fierro, J.L.G. Optimization of the Process of Chemical Hydrolysis of Cellulose to Glucose. *Cellulose* **2014**, *21*, 2397–2407. [CrossRef]
33. Van Putten, R.-J.; van der Waal, J.C.; de Jong, E.; Rasrendra, C.B.; Heeres, H.J.; de Vries, J.G. Hydroxymethylfurfural, A Versatile Platform Chemical Made from Renewable Resources. *Chem. Rev.* **2013**, *113*, 1499–1597. [CrossRef] [PubMed]
34. Sheldon, R.A. Green and Sustainable Manufacture of Chemicals from Biomass: State of the Art. *Green Chem.* **2014**, *16*, 950–963. [CrossRef]
35. Zang, H.; Wang, K.; Zhang, M.; Xie, R.; Wang, L.; Chen, E.Y.-X. Catalytic Coupling of Biomass-Derived Aldehydes into Intermediates for Biofuels and Materials. *Catal. Sci. Technol.* **2018**, *8*, 1777–1798. [CrossRef]
36. Kucherov, F.A.; Romashov, L.V.; Galkin, K.I.; Ananikov, V.P. Chemical Transformations of Biomass-Derived C6-Furanic Platform Chemicals for Sustainable Energy Research, Materials Science, and Synthetic Building Blocks. *ACS Sustain. Chem. Eng.* **2018**, *6*, 8064–8092. [CrossRef]
37. De Jong, E.; Dam, M.A.; Sipos, L.; Gruter, G.-J.M. Furandicarboxylic Acid (FDCA), A Versatile Building Block for a Very Interesting Class of Polyesters. In *ACS Symposium Series*; Smith, P.B., Gross, R.A., Eds.; American Chemical Society: Washington, DC, USA, 2012; Volume 1105, pp. 1–13. ISBN 978-0-8412-2767-5.
38. Eerhart, A.J.J.E.; Faaij, A.P.C.; Patel, M.K. Replacing Fossil Based PET with Biobased PEF: Process Analysis, Energy and GHG Balance. *Energy Environ. Sci.* **2012**, *5*, 6407. [CrossRef]

39. Tsanaktsis, V.; Papageorgiou, G.Z.; Bikiaris, D.N. A Facile Method to Synthesize High-Molecular-Weight Biobased Polyesters from 2,5-Furandicarboxylic Acid and Long-Chain Diols. *J. Polym. Sci. Part Polym. Chem.* **2015**, *53*, 2617–2632. [CrossRef]
40. Papageorgiou, G.Z.; Papageorgiou, D.G.; Terzopoulou, Z.; Bikiaris, D.N. Production of Bio-Based 2,5-Furan Dicarboxylate Polyesters: Recent Progress and Critical Aspects in Their Synthesis and Thermal Properties. *Eur. Polym. J.* **2016**, *83*, 202–229. [CrossRef]
41. Ait Rass, H.; Essayem, N.; Besson, M. Selective Aerobic Oxidation of 5-HMF into 2,5-Furandicarboxylic Acid with Pt Catalysts Supported on TiO_2^- and ZrO_2^- Based Supports. *ChemSusChem* **2015**, *8*, 1206–1217. [CrossRef] [PubMed]
42. Ventura, M.; Nocito, F.; de Giglio, E.; Cometa, S.; Altomare, A.; Dibenedetto, A. Tunable Mixed Oxides Based on CeO_2 for the Selective Aerobic Oxidation of 5-(Hydroxymethyl)Furfural to FDCA in Water. *Green Chem.* **2018**, *20*, 3921–3926. [CrossRef]
43. German, D.; Pakrieva, E.; Kolobova, E.; Carabineiro, S.A.C.; Stucchi, M.; Villa, A.; Prati, L.; Bogdanchikova, N.; Cortés Corberán, V.; Pestryakov, A. Oxidation of 5-Hydroxymethylfurfural on Supported Ag, Au, Pd and Bimetallic Pd-Au Catalysts: Effect of the Support. *Catalysts* **2021**, *11*, 115. [CrossRef]
44. Lolli, A.; Albonetti, S.; Utili, L.; Amadori, R.; Ospitali, F.; Lucarelli, C.; Cavani, F. Insights into the Reaction Mechanism for 5-Hydroxymethylfurfural Oxidation to FDCA on Bimetallic Pd–Au Nanoparticles. *Appl. Catal. Gen.* **2015**, *504*, 408–419. [CrossRef]
45. Albonetti, S.; Pasini, T.; Lolli, A.; Blosi, M.; Piccinini, M.; Dimitratos, N.; Lopez-Sanchez, J.A.; Morgan, D.J.; Carley, A.F.; Hutchings, G.J.; et al. Selective Oxidation of 5-Hydroxymethyl-2-Furfural over TiO_2-Supported Gold–Copper Catalysts Prepared from Preformed Nanoparticles: Effect of Au/Cu Ratio. *Catal. Today* **2012**, *195*, 120–126. [CrossRef]
46. Casanova, O.; Iborra, S.; Corma, A. Biomass into Chemicals: Aerobic Oxidation of 5-Hydroxymethyl-2-Furfural into 2,5-Furandicarboxylic Acid with Gold Nanoparticle Catalysts. *ChemSusChem* **2009**, *2*, 1138–1144. [CrossRef]
47. Monti, E.; Ventimiglia, A.; Forster, L.; Rodríguez-Aguado, E.; Cecilia, J.A.; Ospitali, F.; Tabanelli, T.; Albonetti, S.; Cavani, F.; Rivalta, I.; et al. Influence of Stabilisers on the Catalytic Activity of Supported Au Colloidal Nanoparticles for the Liquid Phase Oxidation of Glucose to Glucaric Acid: Understanding the Catalyst Performance from NMR Relaxation and Computational Studies. *Green Chem.* **2023**, *25*, 2640–2652. [CrossRef]
48. Scurti, S.; Allegri, A.; Liuzzi, F.; Rodríguez-Aguado, E.; Cecilia, J.A.; Albonetti, S.; Caretti, D.; Dimitratos, N. Temperature-Dependent Activity of Gold Nanocatalysts Supported on Activated Carbon in Redox Catalytic Reactions: 5-Hydroxymethylfurfural Oxidation and 4-Nitrophenol Reduction Comparison. *Catalysts* **2022**, *12*, 323. [CrossRef]
49. Scurti, S.; Monti, E.; Rodríguez-Aguado, E.; Caretti, D.; Cecilia, J.A.; Dimitratos, N. Effect of Polyvinyl Alcohol Ligands on Supported Gold Nano-Catalysts: Morphological and Kinetics Studies. *Nanomaterials* **2021**, *11*, 879. [CrossRef]
50. Monti, E.; Ventimiglia, A.; Garcia Soto, C.A.; Martelli, F.; Rodríguez-Aguado, E.; Cecilia, J.A.; Sadier, A.; Ospitali, F.; Tabanelli, T.; Albonetti, S.; et al. Effect of the Colloidal Preparation Method for Supported Preformed Colloidal Au Nanoparticles for the Liquid Phase Oxidation of 1,6-Hexanediol to Adipic Acid. *Catalysts* **2022**, *12*, 196. [CrossRef]
51. Monti, E.; Ventimiglia, A.; Soto, C.A.G.; Martelli, F.; Rodríguez-Aguado, E.; Cecilia, J.A.; Maireles-Torres, P.; Ospitali, F.; Tabanelli, T.; Albonetti, S.; et al. Oxidative Condensation/Esterification of Furfural with Ethanol Using Preformed Au Colloidal Nanoparticles. Impact of Stabilizer and Heat Treatment Protocols on Catalytic Activity and Stability. *Mol. Catal.* **2022**, *528*, 112438. [CrossRef]
52. Albonetti, S.; Lolli, A.; Morandi, V.; Migliori, A.; Lucarelli, C.; Cavani, F. Conversion of 5-Hydroxymethylfurfural to 2,5-Furandicarboxylic Acid over Au-Based Catalysts: Optimization of Active Phase and Metal–Support Interaction. *Appl. Catal. B Environ.* **2015**, *163*, 520–530. [CrossRef]
53. Davis, S.E.; Zope, B.N.; Davis, R.J. On the Mechanism of Selective Oxidation of 5-Hydroxymethylfurfural to 2,5-Furandicarboxylic Acid over Supported Pt and Au Catalysts. *Green Chem.* **2012**, *14*, 143–147. [CrossRef]
54. Megías-Sayago, C.; Lolli, A.; Ivanova, S.; Albonetti, S.; Cavani, F.; Odriozola, J.A. Au/Al_2O_3—Efficient Catalyst for 5-Hydroxymethylfurfural Oxidation to 2,5-Furandicarboxylic Acid. *Catal. Today* **2019**, *333*, 169–175. [CrossRef]
55. Megías-Sayago, C.; Lolli, A.; Bonincontro, D.; Penkova, A.; Albonetti, S.; Cavani, F.; Odriozola, J.A.; Ivanova, S. Effect of Gold Particles Size over Au/C Catalyst Selectivity in HMF Oxidation Reaction. *ChemCatChem* **2020**, *12*, 1177–1183. [CrossRef]
56. Zhao, Y.; Jia, L.; Medrano, J.A.; Ross, J.R.H.; Lefferts, L. Supported Pd Catalysts Prepared via Colloidal Method: The Effect of Acids. *ACS Catal.* **2013**, *3*, 2341–2352. [CrossRef]
57. Tierney, G.F.; Alijani, S.; Panchal, M.; Decarolis, D.; de Gutierrez, M.B.; Mohammed, K.M.H.; Callison, J.; Gibson, E.K.; Thompson, P.B.J.; Collier, P.; et al. Controlling the Production of Acid Catalyzed Products of Furfural Hydrogenation by Pd/TiO_2. *ChemCatChem* **2021**, *13*, 5121–5133. [CrossRef]
58. Van Den Bossche, M. DFTB-Assisted Global Structure Optimization of 13- and 55-Atom Late Transition Metal Clusters. *J. Phys. Chem. A* **2019**, *123*, 3038–3045. [CrossRef]
59. Megías-Sayago, C.; Bonincontro, D.; Lolli, A.; Ivanova, S.; Albonetti, S.; Cavani, F.; Odriozola, J.A. 5-Hydroxymethyl-2-Furfural Oxidation Over Au/Ce_xZr_1-XO_2 Catalysts. *Front. Chem.* **2020**, *8*, 461. [CrossRef]
60. Cramer, C.J. *Essentials of Computational Chemistry: Theories and Models*; John Wiley & Sons: Hoboken, NJ, USA, 2013; ISBN 978-1-118-71227-6.
61. Stephens, P.J.; Devlin, F.J.; Chabalowski, C.F.; Frisch, M.J. Ab Initio Calculation of Vibrational Absorption and Circular Dichroism Spectra Using Density Functional Force Fields. *J. Phys. Chem.* **1994**, *98*, 11623–11627. [CrossRef]
62. McLean, A.D.; Chandler, G.S. Contracted Gaussian Basis Sets for Molecular Calculations. I. Second Row Atoms, $Z = 11–18$. *J. Chem. Phys.* **1980**, *72*, 5639–5648. [CrossRef]

63. Frisch, M.J.; Trucks, G.W.; Schlegel, H.B.; Scuseria, G.E.; Robb, M.A.; Cheeseman, J.R.; Scalmani, G.; Barone, V.; Petersson, G.A.; Nakatsuji, H. *Gaussian 16, Revision C. 01*; Gaussian, Inc.: Wallingford, CT, USA, 2016.
64. Barone, V.; Cossi, M. Quantum Calculation of Molecular Energies and Energy Gradients in Solution by a Conductor Solvent Model. *J. Phys. Chem. A* **1998**, *102*, 1995–2001. [CrossRef]
65. Pritchard, B.P.; Altarawy, D.; Didier, B.; Gibson, T.D.; Windus, T.L. New Basis Set Exchange: An Open, Up-to-Date Resource for the Molecular Sciences Community. *J. Chem. Inf. Model.* **2019**, *59*, 4814–4820. [CrossRef] [PubMed]
66. Schäfer, A.; Horn, H.; Ahlrichs, R. Fully Optimized Contracted Gaussian Basis Sets for Atoms Li to Kr. *J. Chem. Phys.* **1992**, *97*, 2571–2577. [CrossRef]
67. Jansen, H.B.; Ros, P. Calculations Monoxide. *Chem. Phys. Lett.* **1969**, *3*, 140–143. [CrossRef]